Applied Surface Science 556 (2021) 149709

Contents lists available at ScienceDirect

Applied Surface Science

journal homepage: www.elsevier.com/locate/apsusc

Full Length Article

Empowering hydrogen storage properties of haeckelite monolayers via metal atom functionalization

Zhiyang Liu [a,1], Tanveer Hussain [b,c,1], Amir Karton [b], Süleyman Er [d,e,*]

[a] Wuhan National Laboratory for Optoelectronics, Huazhong University of Science and Technology, Wuhan 430074, China
[b] School of Molecular Sciences, The University of Western Australia, Perth, WA 6009, Australia
[c] School of Chemical Engineering, The University of Queensland, St Lucia, QLD 4072, Australia
[d] DIFFER – Dutch Institute for Fundamental Energy Research, De Zaale 20, 5612 AJ Eindhoven, the Netherlands
[e] CCER – Center for Computational Energy Research, De Zaale 20, 5612 AJ Eindhoven, the Netherlands

ARTICLE INFO

Keywords:
Hydrogen storage
Density functional theory calculations
Energy storage materials
2D Materials
Haeckelites

ABSTRACT

Using hydrogen as an energy carrier requires new technological solutions for its onboard storage. The exploration of two-dimensional (2D) materials for hydrogen storage technologies has been motivated by their open structures, which facilitates fast hydrogen kinetics. Herein, the hydrogen storage properties of lightweight metal functionalized r_{57} haeckelite sheets are studied using density functional theory (DFT) calculations. H_2 molecules are adsorbed on pristine r_{57} via physisorption. The hydrogen storage capacity of r_{57} is improved by decorating it with alkali and alkaline-earth metals. In addition, the in-plane substitution of r_{57} carbons with boron atoms (B@r_{57}) both prevents the clustering of metals on the surface of 2D material and increases the hydrogen storage capacity by improving the adsorption thermodynamics of hydrogen molecules. Among the studied compounds, B@r_{57}-Li_4, with its 10.0 wt% H_2 content and 0.16 eV/H_2 hydrogen binding energy, is a promising candidate for hydrogen storage applications. A further investigation, as based on the calculated electron localization functions, atomic charges, and electronic density of states, confirm the electrostatic nature of interactions between the H_2 molecules and the protruding metal atoms on 2D haeckelite sheets. All in all, this work contributes to a better understanding of pure carbon and B-doped haeckelites for hydrogen storage.

1. Introduction

The mounting demands of energy due to increase in population and urbanization have put significant stress on conventional energy sources. Additionally, an increasing use of the fossil fuel-based energy sources has a devastating impact on the environment [1]. This situation calls for clean, renewable, and economically viable energy alternatives that would replace fossil fuels. Hydrogen stands out as a highly promising option due to its high energy density by mass, moreover its abundance, clean and renewable production [2,3]. However, the efficient storage of hydrogen molecules (H_2) is a major bottleneck for the practical use of this, otherwise ideal energy carrier. Conventional H_2 storage methods, such as the pressurized gas and liquefaction, are associated with safety concerns and large energy consumption, respectively [4,5]. Hydrogen can be stored in the lattice or at the surface of host storage materials [6–11]. However, it's an ongoing challenge to find good materials that are capable of storing practically meaningful volumetric and gravimetric amounts of hydrogens and releasing them on demand.

Among the various available options, carbonous materials possess a great potential for H_2 storage applications due to their salient features like stability, cost-effectiveness, and porosity. H_2 storage capacities of the host carbonous materials are further enhanced by increasing their surface areas such as via nanostructuring [12]. However, a downside of carbonous nanostructures is their weak, van der Waals type interactions with the incident H_2 molecules, which allows for molecule storage only at very low temperatures [13–15]. For ambient condition storage applications, the binding energies of H_2 to the host material should be close to 0.16 eV/H_2 [16,17]. To enhance the interactions between H_2 and the host carbonous nanostructures, among the different strategies, the introduction of dopant atoms has been applied with promise [18–22].

In literature, several studies have been devoted to the study of H_2 storage properties of the metalized carbonous nanostructures,

* Corresponding author at: DIFFER – Dutch Institute for Fundamental Energy Research, De Zaale 20, 5612 AJ Eindhoven, the Netherlands.
E-mail address: s.er@differ.nl (S. Er).
[1] These authors contributed equally.

https://doi.org/10.1016/j.apsusc.2021.149709
Received 12 January 2021; Received in revised form 26 March 2021; Accepted 29 March 2021
Available online 15 April 2021

particularly the 2D monolayers [23–26]. A recent study explored the potential of metal-doped nitrogenated holey graphene (C_2N) as H_2 storage material [27]. The authors employed dispersion-corrected DFT simulations to study the adsorption of H_2 molecules on C_2N in its pristine and metal-decorated (e.g. Mg, Ca, Ti, V, Mn, Fe, Co, Ni, and Zn) forms. It was found that the pristine C_2N's weak hydrogen binding energy (0.10 eV/H_2) is enhanced significantly after its decoration with metals. In another study, Chen et al. employed first-principles DFT calculations for the study of lithium functionalized graphitic carbon nitride (g-CN) monolayers for H_2 storage [16]. They found that the Li atoms are strongly bonded to g-CN sheets without being clustered, therefore facilitating a rather uniform distribution of metal cations over the host material. Each Li^+ cation interacted with multiple H_2 molecules and that resulted in a H_2 storage capacity of 10.8 wt% Hydrogen, which is larger than is possible for many other 2D systems, such as phosphorene and MoS_2. Similarly, Faye et al. has recently reported the H_2 storage properties of 2D carbon nitride, C_3N, sheets through spin-polarized DFT simulations [28]. The structural and H_2 adsorption properties of Si- and Ti-doped C_3N nanosheets were studied in the context of ambient condition H_2 storage. They found that the metal-doped C_3N nanosheets were able to reach a high H_2 storage capacity of 9.0 wt% Hydrogen. In addition to the above-mentioned theoretical reports, several experimental groups studied the potential of use different nanomaterials for H_2 storage applications. In this regard, porous carbon-based structures [29,30], multilayered graphene [31] and Ti_2CT_x [32] have recently been explored.

Motivated by the promise of peculiar carbonous nanostructures as discussed in the above studies, we employed DFT calculations to study the structural features and H_2 storage properties of lightweight metal functionalized haeckelites (r_{57}). We found that, the graphene-like open structure, but with 5- and 7-membered rings of carbon atoms, of the haeckelites enable strong interactions with metal adatoms, and they consequently attain good H_2 storage properties.

2. Computational methods

All DFT calculations were carried out using the generalized gradient approximation (GGA) exchange-correlation functional of Perdew-Burke-Ernzerhof (PBE) [33] and the projector augmented wave (PAW) [34,35] method, as implemented in the Vienna *ab initio* simulation package (VASP) [36–38]. A plane wave basis with a kinetic energy cutoff of 600 eV was used. The H 1*s*, B 2*s*2*p*, C 2*s*2*p*, Li 1*s*2*s*, Na 3*s*2*p*, K 3*s*3*p*4*s*, Ca 3*s*3*p*4*s*, Sc 3*p*4*s*3*d* and Ti 3*p*4*s*3*d* electrons were considered as valence. Spin-polarized calculations were performed within the framework of DFT and no charge or dipole correction procedures were applied [39]. The DFT-D3 scheme [40,41] was used to account for the dispersion interactions, which provides accurate results for molecule storage systems [42–45].

The original structural parameters of r_{57} were obtained from literature [46] and the structure was further optimized with the above settings and a vacuum spacing of 20 Å to avoid interactions between periodic images. Using the Γ-centred Monkhorst–Pack scheme [47] with a $7 \times 9 \times 1$ *k*-mesh for the unit cell, the geometries were fully optimized until the total forces acting on each atom were smaller than 0.01 eV/Å. The isolated H_2 molecule was calculated by using a 20 Å edge cubic box with periodicity.

We calculated the binding energy of metal atoms to the host sheet, as follows

$$E_b^M = (nE_M + E_{Host} - E_{Host-M_n})/n \quad (1)$$

where E_M is the total energy of one metal atom in its respective metal crystal, E_{Host} and E_{Host-M_n} are the total energies of the host simulation cells prior and posterior to metal decoration, respectively.

The average adsorption energy (E_{avg}) and the consecutive adsorption energy (E_{con}) of H_2 molecules to the host materials were defined as

$$E_b^{H_2-avg} = (nE_{H_2} + E_{Host} - E_{Host-H_{2n}})/n \quad (2)$$

$$E_b^{H_2-con} = E_{H_2} + E_{Host-H_{2(n-1)}} - E_{Host-H_{2n}} \quad (3)$$

where E_{H_2} is the total energy of a H_2 molecule in gas phase, $E_{Host-H_{2(n-1)}}$ and $E_{Host-H_{2n}}$ are the total energies of the host sheets with $(n-1)$ and n H_2 molecules, respectively.

3. Results and discussions

The optimized structure of the r_{57} monolayer is shown in Fig. 1(a). The optimized lattice constants of the unit cell are $a = 7.47$ and $b = 5.86$ Å, with the C–C bond lengths altering between 1.39 and 1.49 Å. These parameters agree well with the literature [46].

To investigate the interaction of H_2 with the r_{57} sheet, four different kinds of adsorption sites were considered: top of C atoms (C_T), top of C–C bonds (C_B), top of 5-atom ring centres (F_T), and top of 7-atom ring centres (S_T). The lowest energy configuration is found to be when the H_2 molecules are positioned at S_T sites, with $E_b^{H_2} = 0.07$ eV, which indicates a weak interaction between the 2D material and H_2 molecules. For efficient hydrogen storage, the binding interactions of hydrogen molecules on pure r_{57} sheets would have to be improved, such as through the incorporation of lightweight metal atoms to the host material.

Similar to the procedure for hydrogen molecules interacting with the 2D material, for the metal atoms, we also considered different adsorption sites on the r_{57} sheet. For all metals, the lowest energy adsorption site is predicted to be the S_T site and the calculated binding energies of the metal atoms on r_{57} are shown in Table 1. The E_b^M for Li, Na, and K is positive, meaning that these alkali metals adsorb stably on the r_{57} sheet, whereas Ca decoration is prone to metal clustering as evident from the negative E_b^M. Next, we focus on the most promising alkali metal loadings of r_{57}-Li_1, r_{57}-Na_1, and r_{57}-K_1 as host materials for H_2 molecules. The optimized structures prior and posterior to full hydrogen loading are shown in Fig. 2. We found that each Li, Na, and K on r_{57} interact with three H_2 molecules with $E_b^{H_2-avg}$ of 0.18, 0.19, and 0.18 eV/H_2, respectively. On r_{57}-Li_1, a fourth H_2 molecule is accommodated with a moderate E_{con} of 0.13 eV/H_2. However, as shown in Fig. 2(a), it is positioned relatively further away from the Li atom. Similarly, the fourth H_2 molecule binds with E_{con} of 0.16 and 0.12 eV/H_2 on r_{57}-Na_1 and r_{57}-K_1, respectively. The fifth H_2 molecule adsorbs onto the metal atoms of r_{57}-Na_1 (Fig. 2(b)) and r_{57}-K_1 (Fig. 2(c)), but only via weak interactions of 0.08 eV/H_2 and 0.06 eV/H_2, respectively. For all these considered cases of alkali metal modified matrix, the maximum effective hydrogen storage capacity is 3.6 wt% H_2 (for r_{57}-Na_1H_8), which is lower than the 5.5 wt% storage target as set by the U. S. Department of Energy (DOE) [48].

To enhance the hydrogen storage capacity of r_{57} sheets, an increased amount of dispersed metal ions is required on their surface. Earlier theoretical studies show that incorporating B atoms into graphene provides a way for immobilizing metal atoms on its surface [49]. Additionally, taking into account that B-doped graphene monolayers are experimentally realized [50], we also study here the B doping of r_{57}. All the three unique C atoms of r_{57} unit cell, as illustrated in Fig. 1(a), were considered in turn for the atomic substitutions with B. The most stable

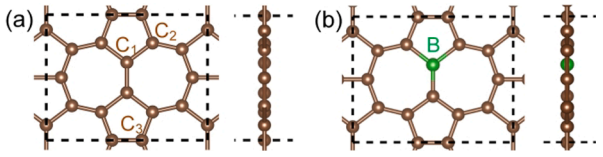

Fig. 1. The top and side views of DFT optimized (a) r_{57} and (b) B@r_{57} unit cells. Brown and green spheres represent C and B atoms, respectively. (For interpretation of the references to colour in this figure legend, the reader is referred to the web version of this article.)

Table 1
The calculated binding energies (E_b^M) of metal atoms on host materials, r_{57} and B@r_{57}, under different metal loading conditions. All units are given in eV/M.

Host	E_b^{Li}	E_b^{Na}	E_b^{K}	E_b^{Ca}
r_{57}-M_1	0.31	0.08	0.65	−0.06
r_{57}-M_4	−0.16	−0.14	0.41	−0.08
r_{57}-M_8	−0.28	−0.05	−0.19	−0.30
B@r_{57}-M_1	0.86	0.57	1.06	0.50
B@r_{57}-M_4	0.20	0.09	0.61	0.20
B@r_{57}-M_8	0.02	0.08	0.06	0.23

configuration, B@r_{57}, is reached when a B atom substitutes C_1 atom, as shown in Fig. 1(b). Next, we studied the adsorption of a H_2 molecule on B@r_{57}, and found that the molecule tends to reside at S_T site with a binding energy of 0.07 eV/H_2, which is both positionally and energetically very similar to the hydrogen molecule on the pure r_{57} sheet.

The calculated adsorption energies of different metal atoms on B@r_{57} are shown in Table 1. According to these results, when compared with r_{57}, the B@r_{57} has stronger interactions with the metal atoms. Interestingly, all metal atoms at any of the considered loading ratios in the current study, have positive binding energies on B@r_{57}. Furthermore, according to Bader charge analysis results of the B@r_{57}-M_n compounds (M = Li, Na, K, and Ca; n = 1, 4, and 8), shown in Table 2, all metal atoms on B@r_{57} monolayers were depleted. However, with an increase in the number of adsorbed metal atoms in the simulation cell, the average electrical charge of metal atoms decreased. Among the metals studied here, the change of charge depletion was lowest for Li, meaning that, Li atoms were electrically the least affected by an increase in metal population on B@r_{57} monolayers.

Next, we discuss the hydrogen storage performances of the M-decorated B@r_{57} sheets.

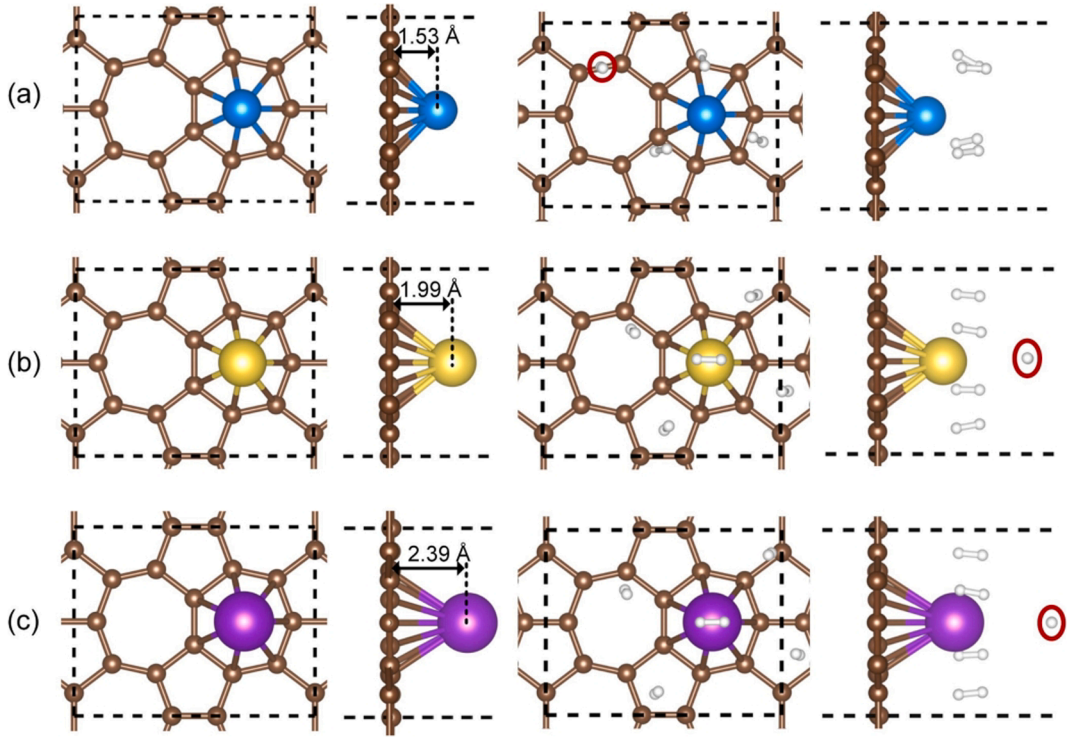

Fig. 2. The most stable structures of r_{57}-M_1 and r_{57}-M_1H_{2n}, where M is (a) Li, (b) Na and (c) K. Brown, blue, golden, purple and white spheres represent C, Li, Na, K, and H atoms, respectively. For clarity, on each compound, the relatively weakly binding H_2 molecules, which have the lowest E_{con} and are furthest away from the metal atoms, have been encircled. (For interpretation of the references to colour in this figure legend, the reader is referred to the web version of this article.)

Table 2
Bader charge (Q) analysis for the constituting atoms of B@r_{57}-M_n compounds, with an increasing number (n) of adsorbed metal atoms. For C and M (=Li, Na, K, Ca) atoms, Q_{ave}, Q_{max} and Q_{min} show respectively the average, maximum and minimum charge variations in absolute values, when compared to the charge neutral states of atoms. Positive and negative values indicate depletion and accumulation of electrical charge on atoms, respectively. All charges are given in units of $|e|$.

Compound	Q^B	Q^C_{ave}	Q^C_{max}	Q^C_{min}	Q^M_{ave}	Q^M_{max}	Q^M_{min}
B@r_{57}	+1.90	−0.13	−0.70	−0.01			
B@r_{57}-Li_1	+1.81	−0.18	−0.83	+0.01	+0.89	+0.89	+0.89
B@r_{57}-Li_4	+1.67	−0.34	−0.91	−0.12	+0.85	+0.85	+0.84
B@r_{57}-Li_8	+1.38	−0.47	−1.31	−0.24	+0.71	+0.75	+0.64
B@r_{57}-Na_1	+1.81	−0.18	−0.81	+0.00	+0.87	+0.87	+0.87
B@r_{57}-Na_4	+1.73	−0.28	−0.87	−0.05	+0.60	+0.60	+0.59
B@r_{57}-Na_8	+1.66	−0.30	−0.90	−0.10	+0.36	+0.47	+0.21
B@r_{57}-K_1	+1.83	−0.18	−0.79	+0.00	+0.85	+0.85	+0.85
B@r_{57}-K_4	+1.77	−0.25	−0.84	−0.06	+0.50	+0.50	+0.49
B@r_{57}-K_8	+1.67	−0.30	−0.84	−0.12	+0.35	+0.40	+0.28
B@r_{57}-Ca_1	+1.78	−0.20	−0.84	−0.01	+1.18	+1.18	+1.18
B@r_{57}-Ca_4	+1.64	−0.35	−0.96	−0.12	+0.89	+0.91	+0.88
B@r_{57}-Ca_8	+1.46	−0.40	−0.98	−0.21	+0.57	+0.77	+0.33

(1) **Li decoration**: For one-, four-, and eight-Li atom decorations, the most stable geometries of the compounds are shown in Fig. 3(a)-(c), with the corresponding E_b^{Li} = 0.86, 0.20, and 0.02 eV/Li, respectively. Considering both E_b^{Li} and sterical suitability for molecular hydrogen interactions, the four-Li atom decorated B@r_{57} compound, B@r_{57}-Li_4, provides a good balance of metal loading for hydrogen storage purposes. To further illustrate the stability of B@r_{57}-Li_4, we carried out *ab initio* molecular dynamics (AIMD) calculations [51] on the corresponding 2 × 2 × 1 supercell. Fig. 4 shows the structures at the end of 10 ps AIMD calculations that were performed at four different temperatures of 200, 300, 400, and 500 K. Although the Li atoms became more mobile with an increase in temperature, they still were attached to the 2D material even at elevated temperatures. Moreover, we studied the cases when each Li attracts one, two, and three H_2 molecules, and found that B@r_{57}-Li_4 efficiently adsorbed a total of 12 H_2 molecules with $E_b^{H_2-avg}$ = 0.16 eV/H_2. Accordingly, the hydrogen storage capacity of B@r_{57}-Li_4 reached to 10.0 wt% H_2.

(2) **Na/K decoration:** Either of the single Na and K atom decorated B@r_{57} compounds adsorbed four H_2 molecules to the most, with $E_b^{H_2-avg}$ = 0.17 eV/H_2 and 0.14 eV/H_2, respectively. For four-Na or four-K decorated B@r_{57}, the interactions between H_2 molecules and Na/K surface atoms were weak (e.g.$E_b^{H_2-avg}$ = 0.08 eV/H_2 for B@r_{57}-Na_4H_8). These results were in relation to the relatively inefficient discharge of these atoms (Q_{ave}^{Na} = +0.60 |*e*|, Q_{ave}^{K}= +0.50 |*e*|) after their deposition onto the B@r_{57} monolayers.

(3) **Ca decoration:** The Ca atom of the B@r_{57}-Ca_1 compound effectively adsorbed up to five H_2 molecules with $E_b^{H_2-avg}$ = 0.21 eV/H_2. However, when the number of Ca atoms increased to four to form the B@r_{57}-Ca_4 compound, then each Ca interacted with a maximum of four H_2 molecules and with $E_b^{H_2-avg}$ = 0.12 eV/H_2. Nevertheless, this compound still reached to a hydrogen storage capacity of 8.4 wt% H_2.

The metal ions of the B@r_{57}-M_1 compounds interact with only three to five H_2 molecules, whereas for the B@r_{57}-M_8 compounds, the distances between neighbouring metal atoms are comparable to the respective M-M distances found in their bulk metal crystal structures. Additionally, for the latter compounds, the calculated absolute Bader charge values of metal ions were small. Thus, due to steric and electronic effects, these compounds are not the most interesting compositions for hydrogen storage. Based on these findings, the B@r_{57}-Li_4 compound is the most promising candidate for molecular hydrogen storage. Therefore, to provide a versatile insight into the nature of interactions between H_2 molecules and B@r_{57}-Li_4, we further studied their electronic properties.

Fig. 5 shows the optimized geometry of the fully hydrogen loaded B@r_{57}-Li_4H_{24} compound and its corresponding electron localization function (ELF), both as calculated using DFT. Clearly, all Li atoms were exposed on the B@r_{57} monolayer and they were electrically depleted.

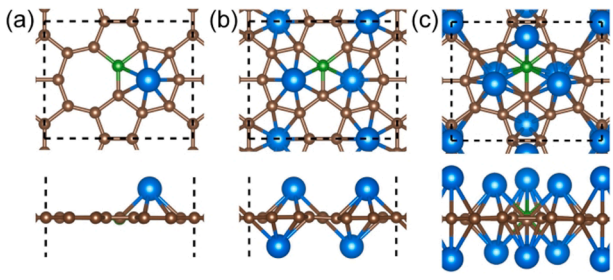

Fig. 3. The top and side views of the DFT optimized structures of (a) B@r_{57}-Li_1, (b) B@r_{57}-Li_4, and (c) B@r_{57}-Li_8 compounds.

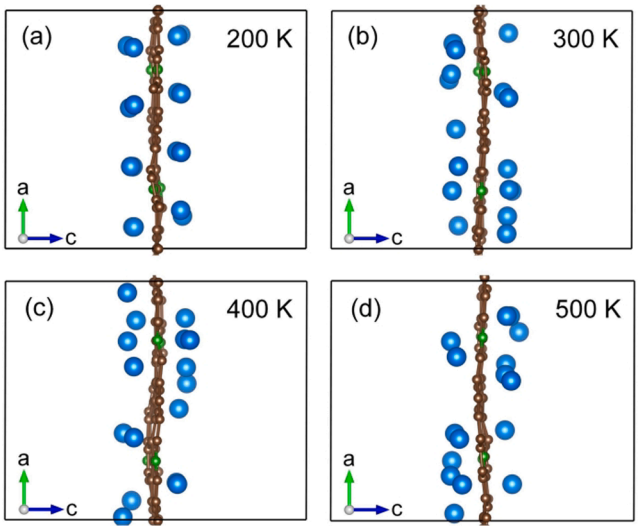

Fig. 4. The snapshots from the side view of the 2 × 2 × 1 B@r_{57}-Li_4 supercell, as obtained at the end of 10 ps AIMD simulations at T = 200, 300, 400, and 500 K, respectively from (a) to (d).

Moreover, Li atoms had no apparent orbital interactions with either of the B@r_{57} monolayer or the H_2 molecules that were positioned around them. The localized electron clouds surrounding the H_2 molecules showed no evidence of orbital interactions with the atoms of the host material. The electronic density of states (DOS) calculations were also used to investigate the B@r_{57}-Li_4 compounds. As shown in Fig. 6(a) DOS plot of the pure B@r_{57} monolayer, the bonding contributions were mainly from the *p* orbitals of C and B atoms. When Li dopants were added onto the monolayer, their valance *s* electrons were transferred to the host material and no strong orbital interactions were evident between Li and monolayer C or B atoms (Fig. 6(b)). Instead, the charge transfer from Li atoms to the 2D material results in an increased density for the occupied states of C and B atoms, which indicates ionic bonding between the metal and nonmetal atoms of B@r_{57}-Li_4. Fig. 6(c) shows the DOS for the fully hydrogenated B@r_{57}-Li_4 compound. The adsorbed H_2 molecules on the monolayer populate around −9 eV, and they showed no real influence on the valance states of C, B, and Li atoms. The calculated DOS data is consistent with the above discussed ELF and atomic charge analysis results.

4. Conclusions

In summary, the adsorption of H_2 molecules on lightweight metal atom decorated haeckelites was studied by first-principles DFT calculations. We found that H_2 molecules interact weakly with pristine r_{57} and B-doped B@r_{57} haeckelites. With the introduction of alkali and alkaline earth metals, the binding energies of hydrogen molecules were improved. When compared with pure r_{57}, the B@r_{57} haeckelites were more useful in immobilizing the metal atoms, and hence more successful in reaching to high hydrogen storage capacities. Of the metal decorated B@r_{57} systems investigated here, the B@r_{57}-Li_4 compound is the most promising candidate for practical usage, as it yielded the highest hydrogen storage capacity of 10.0 wt% H_2 at a hydrogen binding energy of 0.16 eV/H_2. A further analysis of the electronic structures revealed that the interactions between the protruding Li atoms of the B@r_{57}-Li_4 compound and the H_2 molecules were mainly electrostatic by nature.

CRediT authorship contribution statement

Zhiyang Liu: Conceptualization, Methodology, Formal analysis, Funding acquisition, Visualization, Writing - review & editing. **Tanveer Hussain:** Conceptualization, Methodology, Formal analysis, Writing -

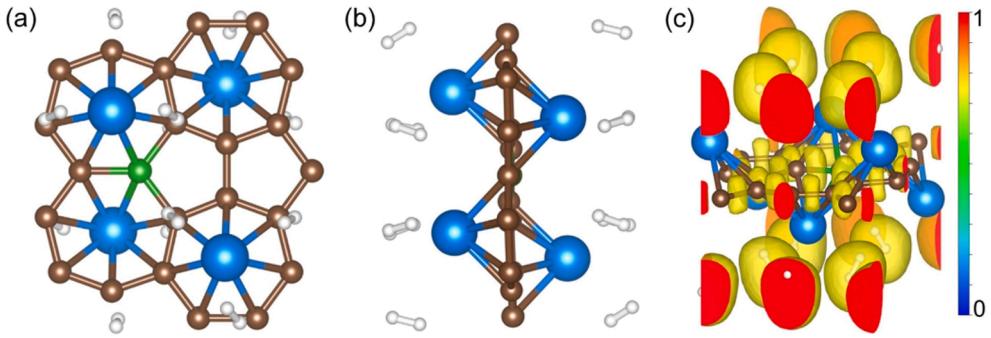

Fig. 5. The DFT optimized structure of B@r_{57}-Li_4H_{24}, as shown from (a) top and (b) side views, and (c) its ELF as shown from a perspective view.

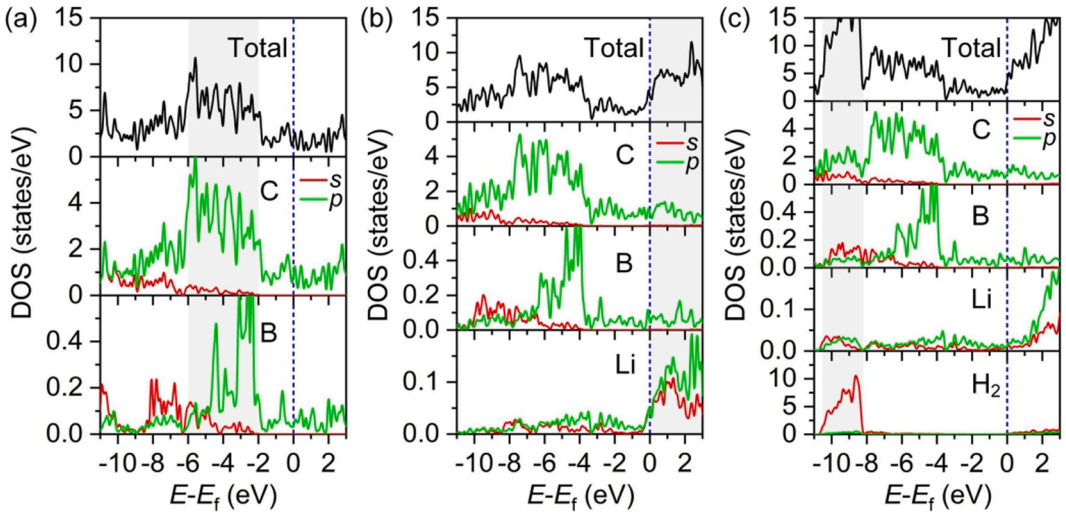

Fig. 6. The DFT calculated total and local electronic DOS for the compounds (a) B@r_{57}, (b) B@r_{57}-Li_4, and (c) B@r_{57}-Li_4H_{24}. For the local DOS, the *s* and *p* orbital contributions, as projected onto atoms, were shown in red and green, respectively. The origin of the energy scale was set at the Fermi level and shown with vertical dashed lines.

review & editing. **Amir Karton:** Funding acquisition, Writing - review & editing. **Süleyman Er:** Conceptualization, Methodology, Funding acquisition, Supervision, Writing - review & editing.

Declaration of Competing Interest

The authors declare that they have no known competing financial interests or personal relationships that could have appeared to influence the work reported in this paper.

Acknowledgements

ZL acknowledges the Fund of Post-doctoral Innovation Research Post (Grant No. 0106187143). AK acknowledges an Australian Research Council (ARC) Future Fellowship (FT170100373). SE acknowledges funding from the initiative "Computational Sciences for Energy Research" of Shell and NWO (Grant No. 15CSTT05). This work was sponsored by NWO Exact and Natural Sciences for the use of supercomputer facilities. The authors gratefully acknowledge the assistance of Dr. Zewen Xiao, Huazhong University of Science and Technology in simulation.

References

[1] G. Nicoletti, N. Arcuri, G. Nicoletti, R. Bruno, A technical and environmental comparison between hydrogen and some fossil fuels, Energy Convers. Manage. 89 (2015) 205–213, https://doi.org/10.1016/j.enconman.2014.09.057.

[2] K. Alhameedi, T. Hussain, H. Bae, D. Jayatilaka, H. Lee, A. Karton, Reversible hydrogen storage properties of defect-engineered C_4N nanosheets under ambient conditions, Carbon N. Y. 152 (2019) 344–353, https://doi.org/10.1016/j.carbon.2019.05.080.

[3] S. Dutta, A review on production, storage of hydrogen and its utilization as an energy resource, J. Ind. Eng. Chem. 20 (2014) 1148–1156, https://doi.org/10.1016/j.jiec.2013.07.037.

[4] U. Eberle, M. Felderhoff, F. Schüth, Chemical and physical solutions for hydrogen storage, Angew. Chemie Int. Ed. 48 (2009) 6608–6630, https://doi.org/10.1002/anie.200806293.

[5] J. Yang, A. Sudik, C. Wolverton, D.J. Siegel, High capacity hydrogen storage materials: attributes for automotive applications and techniques for materials discovery, Chem. Soc. Rev. 39 (2010) 656–675, https://doi.org/10.1039/B802882F.

[6] I. Sreedhar, K.M. Kamani, B.M. Kamani, B.M. Reddy, A. Venugopal, A Bird's Eye view on process and engineering aspects of hydrogen storage, Renew. Sustain. Energy Rev. 91 (2018) 838–860, https://doi.org/10.1016/j.rser.2018.04.028.

[7] T. Hussain, B. Mortazavi, H. Bae, T. Rabczuk, H. Lee, A. Karton, Enhancement in hydrogen storage capacities of light metal functionalized Boron-Graphdiyne nanosheets, Carbon N. Y. 147 (2019) 199–205, https://doi.org/10.1016/j.carbon.2019.02.085.

[8] Z. Liu, S. Liu, S. Er, Hydrogen storage properties of Li-decorated B_2S monolayers: A DFT study, Int. J. Hydrogen Energy. 44 (2019) 16803–16810, https://doi.org/10.1016/j.ijhydene.2019.04.234.

[9] S. Er, G.A. de Wijs, G. Brocks, DFT study of planar boron sheets: a new template for hydrogen storage, J. Phys. Chem. C. 113 (2009) 18962–18967, https://doi.org/10.1021/jp9077079.

[10] S. Er, G.A. de Wijs, G. Brocks, Improved hydrogen storage in Ca-decorated boron heterofullerenes: a theoretical study, J. Mater. Chem. A. 3 (2015) 7710–7714, https://doi.org/10.1039/c4ta06818a.

[11] Y. Wang, G. Xu, S. Deng, Q. Wu, Z. Meng, X. Huang, L. Bi, Z. Yang, R. Lu, Lithium and sodium decorated graphdiyne as a candidate for hydrogen storage: first-principles and grand canonical Monte Carlo study, Appl. Surf. Sci. 509 (2020), 144855, https://doi.org/10.1016/j.apsusc.2019.144855.

[12] Y. Xia, Z. Yang, Y. Zhu, Porous carbon-based materials for hydrogen storage: advancement and challenges, J. Mater. Chem. A. 1 (2013) 9365–9381, https://doi.org/10.1039/C3TA10583K.
[13] P. Panigrahi, A.K. Dhinakaran, S.R. Naqvi, S.R. Gollu, R. Ahuja, T. Hussain, Light metal decorated graphdiyne nanosheets for reversible hydrogen storage, Nanotechnology. 29 (2018), 355401, https://doi.org/10.1088/1361-6528/aac84c.
[14] J.-H. Park, S.-J. Park, Expansion of effective pore size on hydrogen physisorption of porous carbons at low temperatures with high pressures, Carbon N. Y. 158 (2020) 364–371, https://doi.org/10.1016/j.carbon.2019.10.100.
[15] T. Hussain, M. Hankel, D.J. Searles, Graphenylene monolayers doped with alkali or alkaline earth metals: promising materials for clean energy storage, J. Phys. Chem. C. 121 (2017) 14393–14400, https://doi.org/10.1021/acs.jpcc.7b02191.
[16] Y.-D. Chen, S. Yu, W.-H. Zhao, S.-F. Li, X.-M. Duan, A potential material for hydrogen storage: a Li decorated graphitic-CN monolayer, Phys. Chem. Chem. Phys. 20 (2018) 13473–13477, https://doi.org/10.1039/c8cp01145a.
[17] S.K. Bhatia, A.L. Myers, Optimum conditions for adsorptive storage, Langmuir. 22 (2006) 1688–1700, https://doi.org/10.1021/la0523816.
[18] S.R. Naqvi, T. Hussain, W. Luo, R. Ahuja, Metallized siligraphene nanosheets (SiC_7) as high capacity hydrogen storage materials, Nano Res. 11 (2018) 3802–3813, https://doi.org/10.1007/s12274-017-1954-z.
[19] E.V. Anikina, A. Banerjee, V.P. Beskachko, R. Ahuja, Influence of Kubas-type interaction of B-Ni codoped graphdiyne with hydrogen molecules on desorption temperature and storage efficiency, Mater. Today Energy. 16 (2020), 100421, https://doi.org/10.1016/j.mtener.2020.100421.
[20] T. Hussain, M.S. Islam, G.S. Rao, P. Panigrahi, D. Gupta, R. Ahuja, Hydrogen storage properties of light metal adatoms (Li, Na) decorated fluorographene monolayer, Nanotechnology. 26 (2015), 275401, https://doi.org/10.1088/0957-4484/26/27/275401.
[21] P. Mishra, D. Singh, Y. Sonvane, R. Ahuja, Enhancement of hydrogen storage capacity on co-functionalized GaS monolayer under external electric field, Int. J. Hydrogen Energy. 45 (2020) 12384–12393, https://doi.org/10.1016/j.ijhydene.2020.02.186.
[22] M. Shi, L. Bi, X. Huang, Z. Meng, Y. Wang, Z. Yang, Design of three-dimensional nanotube-fullerene-interconnected framework for hydrogen storage, Appl. Surf. Sci. 534 (2020), 147606, https://doi.org/10.1016/j.apsusc.2020.147606.
[23] C. Ataca, E. Aktürk, S. Ciraci, H. Ustunel, High-capacity hydrogen storage by metallized graphene, Appl. Phys. Lett. 93 (2008), 043123, https://doi.org/10.1063/1.2963976.
[24] A. Bhattacharya, S. Bhattacharya, C. Majumder, G.P. Das, Transition-metal decoration enhanced room-temperature hydrogen storage in a defect-modulated graphene sheet, J. Phys. Chem. C. 114 (2010) 10297–10301, https://doi.org/10.1021/jp100230c.
[25] W. Zhang, Z. Zhang, F. Zhang, W. Yang, Ti-decorated graphitic-C_3N_4 monolayer: A promising material for hydrogen storage, Appl. Surf. Sci. 386 (2016) 247–254, https://doi.org/10.1016/j.apsusc.2016.06.019.
[26] T. Hussain, T. Kaewmaraya, M. Hankel, V. Amornkitbamrung, Functionalized carbon nitride (g-CN) monolayer as a promising energy storage material: A density functional theory study, Appl. Surf. Sci. 419 (2017) 708–712, https://doi.org/10.1016/j.apsusc.2017.05.119.
[27] R. Varunaa, P. Ravindran, Potential hydrogen storage materials from metal decorated 2D–C_2N: an ab initio study, Phys. Chem. Chem. Phys. 21 (2019) 25311–25322, https://doi.org/10.1039/C9CP05105H.
[28] O. Faye, T. Hussain, A. Karton, J. Szpunar, Tailoring the capability of carbon nitride (C_3N) nanosheets toward hydrogen storage upon light transition metal decoration, Nanotechnology. 30 (2018) 75404, https://doi.org/10.1088/1361-6528/aaf3ed.
[29] G. Yushin, R. Dash, J. Jagiello, J.E. Fischer, Y. Gogotsi, Carbide-derived carbons: effect of pore size on hydrogen uptake and heat of adsorption, Adv. Funct. Mater. 16 (2006) 2288–2293, https://doi.org/10.1002/adfm.200500830.
[30] W. Hu, J. Huang, P. Yu, M. Zheng, Y. Xiao, H. Dong, Y. Liang, H. Hu, Y. Liu, Hierarchically porous carbon derived from neolamarckia cadamba for electrochemical capacitance and hydrogen storage, ACS Sustain. Chem. Eng. 7 (2019) 15385–15393, https://doi.org/10.1021/acssuschemeng.9b02734.
[31] P.K. Chauhan, V. Vidhukiran, R. Sujith, R. Parameshwaran, Experimental investigation of multilayered graphene systems for hydrogen storage, Mater. Res. Express. 6 (2019), 105617, https://doi.org/10.1088/2053-1591/ab3cdc.
[32] S. Liu, J. Liu, X. Liu, J. Shang, L. Xu, R. Yu, J. Shui, Hydrogen storage in incompletely etched multilayer Ti_2CT_x at room temperature, Nat. Nanotechnol. (2021), https://doi.org/10.1038/s41565-020-00818-8.
[33] J.P. Perdew, K. Burke, M. Ernzerhof, Generalized gradient approximation made simple, Phys. Rev. Lett. 77 (1996) 3865–3868, https://doi.org/10.1103/PhysRevLett.77.3865.
[34] P.E. Blöchl, Projector augmented-wave method, Phys. Rev. B. 50 (1994) 17953–17979, https://doi.org/10.1103/PhysRevB.50.17953.
[35] G. Kresse, D. Joubert, From ultrasoft pseudopotentials to the projector augmented-wave method, Phys. Rev. B. 59 (1999) 1758–1775, https://doi.org/10.1103/PhysRevB.59.1758.
[36] G. Kresse, J. Hafner, Ab initio molecular dynamics for open-shell transition metals, Phys. Rev. B. 48 (1993) 13115, https://doi.org/10.1103/PhysRevB.48.13115.
[37] G. Kresse, J. Furthmuller, Efficiency of ab-initio total energy calculations for metals and semiconductors using a plane-wave basis set, Comput. Mater. Sci. 6 (1996) 15–50, https://doi.org/10.1016/0927-0256(96)00008-0.
[38] G. Kresse, J. Furthmuller, Efficient iterative schemes for ab initio total-energy calculations using a plane-wave basis set, Phys. Rev. B. 54 (1996) 11169–11186, https://doi.org/10.1103/PhysRevB.54.11169.
[39] I. Tezsevin, M.C.M. van de Sanden, S. Er, Surface charging activated mechanism change: a computational study of O, CO, and CO_2 interactions on Ag electrodes, J. Energy Chem. 50 (2020) 307–313, https://doi.org/10.1016/j.jechem.2020.03.080.
[40] S. Grimme, J. Antony, S. Ehrlich, H. Krieg, A consistent and accurate ab initio parametrization of density functional dispersion correction (DFT-D) for the 94 elements H-Pu, J. Chem. Phys. 132 (2010), https://doi.org/10.1063/1.3382344.
[41] S. Grimme, Density functional theory with London dispersion corrections, Wiley Interdiscip. Rev. Comput. Mol. Sci. 1 (2011) 211–228, https://doi.org/10.1002/wcms.30.
[42] C.D. Zeinalipour-Yazdi, J.S.J. Hargreaves, S. Laassiri, C.R.A. Catlow, DFT-D3 study of H_2 and N_2 chemisorption over cobalt promoted Ta_3N_5-(100), (010) and (001) surfaces, Phys. Chem. Chem. Phys. 19 (2017) 11968–11974, https://doi.org/10.1039/c7cp00806f.
[43] F. Silveri, M.G. Quesne, A. Roldan, N.H. De Leeuw, C.R.A. Catlow, Hydrogen adsorption on transition metal carbides: a DFT study, Phys. Chem. Chem. Phys. 21 (2019) 5335–5343, https://doi.org/10.1039/c8cp05975f.
[44] Z. Liu, E. Wu, J. Li, S. Liu, Energy storage properties of a two-dimensional TiB_4 monolayer, Phys. Chem. Chem. Phys. 21 (2019) 13151–13156, https://doi.org/10.1039/C9CP01864F.
[45] R.W. Cross, S.R. Rondiya, N.Y. Dzade, First-principles DFT insights into the adsorption of hydrazine on bimetallic β1-NiZn catalyst: Implications for direct hydrazine fuel cells, Appl. Surf. Sci. 536 (2021), 147648, https://doi.org/10.1016/j.apsusc.2020.147648.
[46] S. Thomas, H. Jung, S. Kim, B. Jun, C.H. Lee, S.U. Lee, Two-dimensional haeckelite h567: A promising high capacity and fast Li diffusion anode material for lithium-ion batteries, Carbon N. Y. 148 (2019) 344–353, https://doi.org/10.1016/j.carbon.2019.03.085.
[47] H.J. Monkhorst, J.D. Pack, Special points for Brillouin-zone integrations, Phys. Rev. B. 13 (1976) 5188–5192, https://doi.org/10.1103/PhysRevB.13.5188.
[48] DOE technical targets for onboard hydrogen storage for light-duty vehicles, 2021. http://www.energy.gov/eere/fuelcells/doe-technical-targets-onboard-hydrogen-storage-light-duty-vehicles.
[49] I.-H. Lin, Y.-J. Tong, H.-J. Hsieh, H.-W. Huang, H.-T. Chen, Hydrogen adsorption and storage in boron-substituted and nitrogen-substituted nano-carbon materials decorated with alkaline earth metals, Int. J. Energy Res. 40 (2016) 230–240, https://doi.org/10.1002/er.3457.
[50] Y. Wu, Z. Han, W. Younas, Y. Zhu, X. Ma, C. Cao, P-type boron-doped monolayer graphene with tunable bandgap for enhanced photocatalytic H_2 evolution under visible-light irradiation, ChemCatChem. 11 (2019) 5145–5153, https://doi.org/10.1002/cctc.201901258.
[51] D. Marc, J. Hutter, Ab Initio Molecular Dynamics: Theory and Implementation, John von Neumann Institute for Computing, Julich, 2000.